Available online at www.CivileJournal.org

Civil Engineering Journal

(E-ISSN: 2476-3055; ISSN: 2676-6957)

Vol. 10, No. 07, July, 2024

The Effect of Oil Contaminated on Collapse Pattern in Gypseous Soil Using Particle Image Velocimetry and Simulation

Hala Mahmood Jawad [1], Zuhair Kadhim Jahanger [2*]

[1] *Department of Civil Engineering, College of Engineering, University of Baghdad, Baghdad 10071, Iraq.*

[2] *Department of Water Resources Engineering, College of Engineering, University of Baghdad, Baghdad 10071, Iraq.*

Received 10 February 2024; Revised 22 June 2024; Accepted 26 June 2024; Published 01 July 2024

Abstract

Gypseous soil covers approximately 30% of Iraqi lands and is widely used in geotechnical and construction engineering as it is. The demand for residential complexes has increased, so one of the significant challenges in studying gypsum soil due to its unique behavior is understanding its interaction with foundations, such as strip and square footing. This is because there is a lack of experiments that provide total displacement diagrams or failure envelopes, which are well-considered for non-problematic soil. The aim is to address a comprehensive understanding of the micromechanical properties of dry, saturated, and treated gypseous sandy soils and to analyze the interaction of strip base with this type of soil using particle image velocimetry (PIV) measurement and Plaxis 3D simulation. The results showed that high-resolution digital cameras captured soil deformation using PIV, displacement fields, and velocity vectors were generated, which helped identify different sand movement zones. Further, PIV showed punching and general shear failure in uncontaminated and soaked contaminated gypsum soils, respectively. Moreover, the Plaxis results corresponded well with the PIV, as material behavior models are essentially simplified representations of the actual behavior of footing and soil. Understanding soil deformation behavior is crucial for accurate engineering calculations and designs, making these findings valuable for geotechnical and construction engineering applications.

Keywords: Collapsible Soil; Kerosene; Particle image velocimetry; Finite Element Method.

1. Introduction

Gypseous soils are prevalent worldwide and make up approximately 30% of Iraq's land [1]. This soil is often stiff when dry, but it becomes weaker when wet due to water leaks or changes in water level that can dissolve the gypsum and result in the production of huge pores. Gypseous soils become more permeable as a result of cavity formation, which causes structures to fail and collapse. Where investigate the suitability of unsaturated gypseous soil under different conditions as machine foundation soil. The study found that the elastic modulus of unsaturated gypseous soil increased with decreasing strain and compressibility at a degree of 60% saturation, and the best results were obtained in terms of strength, but when the soil was at higher saturation levels, the elastic modulus decreased gradually and with the lowest strength, regardless of the load frequency [2].

Generally, gypseous soils have the potential to induce significant deformations in structures or dams, ultimately culminating in their catastrophic collapse, thereby presenting numerous challenges for geotechnical engineers [3]. Consequently, the soil collapses. The behavior and pattern of the untreated and treated saturated gypseous sand soil that affects the foundations' stability were not thoroughly studied. On the other hand, most such studies are focused on

* Corresponding author: zk_jahanger@coeng.uobaghdad.edu.iq

http://dx.doi.org/10.28991/CEJ-2024-010-07-016

the collapse potential percentage [4]. To mitigate the increasing prevalence of the problem of collapsible soil [5], numerous techniques were implemented. To assess the collapse properties of sandy soil containing moderate gypsum content, an experimental model test was devised [6]. The findings indicated that increasing the dry density of the top layer of compaction resulted in a moderate reduction of collapsibility by a certain percentage. A collapsibility settlement reduction factor of up to a medium percent was achieved by combining compaction with water treatment sediment. The other studies investigated the effect of using a skirt with a square foundation on gypseous soil with a high gypsum content, which was found to improve the load-carrying capacity and reduce settlement of the foundation. The amount of improvement increases with increasing skirt depth to foundation width ratio [7].

Here, it is worth mentioning that focus was given to adding additives, admixtures, or correct compaction. The procedure yields more stable soil, which can be used in the field or put to the ground prior to building a structure or placing a load on it. Das [8] showed that improving the soil is typically done to lessen the settling of buildings, boost the soil's shear strength, which will raise the shallow foundation's bearing capability, and raise the safety factor to account for the possibility of earth dam and embankment slope failure. The detrimental effects of water leakage or percolation are effectively mitigated by spreading this improved soil in a finite thickness to create an impermeable covering beneath foundations. Numerous researchers have engaged in the search for an inexpensive and efficient material to enhance gypseous soils. For instance, Al-Zory [9] investigated the stability of lime as a treatment for gypseous soil, whereas Aziz & Ma [10] utilized cement as an improvement material. Bituminous materials are widely recognized as the primary waterproofing agents suitable for gypseous soil [1].

Using PLAXIS 2D, 3D, and comparison with field results, skirted footings were employed to lessen settlement in unstable soil and boost the bearing capacity of shallow foundations. Finite element analysis was used to perform numerical simulations to examine the stability of circular skirted footings on gypseous soil. According to the results of the numerical analysis conducted with Plaxis 2D, sand cushioning with reinforcement was used to be the most effective technique in shear failure and mitigating deformation in soft peat soils. Where stress relief on the peat layer is significantly influenced by the composite compacted cushion with a greater number of cycles and stress [11]. The findings demonstrate that the ultimate bearing capacity and settlement are significantly influenced by the skirt embedment ratio, with higher ratios resulting in better performance [12]. Through their study using Plaxis 2D, the results of the experiment indicate that 0.4% for polypropylene and 0.6% for sugarcane bags is the ideal fiber content for lowering collapse potential, with polypropylene having a higher effectiveness in this regard [13]. Moreover, gypseous soil can be made more bearing capacity by using compacted cement dust (Case 1) or biaxial geogrids to reinforce the soil (Case 2). PLAXIS 2D Professional v.8.2 is used to estimate the footing's ultimate bearing capacity, and the results of the two methods are compared to determine the bearing capacity improvement ratio (BCR).

According to the findings, the ideal geogrid layer shape is N=3, with a depth of 0.3, a width of 4, and a spacing between layers of 0.3. This configuration provides a higher ultimate bearing capacity than utilizing compacted cement dust [14]. It was found that using these products can control the collapse potential and shear strength drop that follows soaking. Since there will be less direct contact between the gypsum particles and the water when such materials are used to treat the gypseous soil, the amount of gypsum that dissolves will be reduced. The kind of admixture material to be used will rely on several factors, such as the following: the kind of soil to be treated, the intended use, the minimum requirement (or specification) of engineering features, the availability of materials, the cost, and any environmental issues. Where apart from traditional admixtures, a plethora of contemporary proprietary chemical additions were developed with an emphasis on environmental conscience, specifically for the purpose of treating and applying these additives to difficult-to-mix and problematic soils. This argument might support the use of petroleum compounds to prevent gypseous soils from collapsing shortly. As previously demonstrated, little is known about how oily soil influences the weight-bearing capacity of weak foundations. Therefore, engineers are better prepared to deal with the particular problems given by gypseous soils in Iraq and elsewhere if PIV is used to analyze the behavior of gypseous soils.

Particle image velocimetry, a non-invasive optical technique, can be used to quantify the velocity fields of both fluids and solids [15]. To better understand the behavior of fluids and solids, PIV was used by several disciplines, including soil mechanics and fluid dynamics. The response of soils to different stressors was studied extensively in recent years using PIV. PIV was employed under interfering square footings to study the failure mechanism and soil deformation pattern [16], and it was shown to be a very useful tool for clarifying soil behavior in a variety of scenarios when Lavasan & Ghazavi [17] used PIV to study the fluid flow around submerged obstacles. Others have used PIV in their research on different subjects regarding geotechnical topics such as footing and piles [18-20]. Also, a comparative PIV study was carried out [21] to examine the granular mechanical characteristics of the interactions between grain and structure in sand soils. The findings showed that the packing density and the kind of loading—quasi-static and cyclic loading, for example—had an impact on the mechanical properties of the soil. Because of this, by better understanding the behavior of gypseous soils through PIV and other methods, engineers may build workable solutions to limit or lessen the negative effects as much as possible. Due to the specific problems posed by haphazard soils, such as those found in Iraq, more research must be done on these soils, and effective engineering solutions must be developed. Civil engineers must take into account the bearing capacity of the soil as well as the effects of soil displacement when designing the building of a structure or a foundation on the soil. While soil displacement effects relate to the deformation of the soil brought on by weight, the carrying capacity of the soil is the maximum load that it can support. Also, a wide range of soil displacements and bearing capabilities were reported in the literature. The association between soil carrying capacity, settlement, compressibility, and shear strength for various soil types is shown by these tests. The importance of considering the potential effects of soil movement on building substructures was also brought out by these investigations [22].

The carrying capacity and collapse susceptibility of gypseous soil were examined using geotextile reinforcement. Soil movement was found to have important consequences. Occasionally, PIV can be used to observe the dynamics of stressed soil. The total displacement diagrams (failure envelope) of gypseous sandy soils in both untreated and treated states interacting with foundations, such as strip and square footing constructions, are currently lacking in studies, nevertheless. To deal with the aforementioned shortcomings in the current literature, the presented study focused on collapse patterns, knowing the settlement and its influence on footing under load. For this purpose, the problem of soil with the foundation was extensively investigated in the current research. To that end, a model of gypseous sand was established to study this effect. A detailed experimental investigation was carried out using PIV analyses performed on images through various loading stages. Moreover, numerical analysis was also executed. Using the finite-element program PLAXIS 3D to extend the study to and comparison between the experimental work. The subsequent section presents specifics of the conducted experiments, a comparison of the outcomes, and a numerical analysis utilizing the finite-element approach.

The experimental and computational study contributes new advancements in the field of soil-footing interactions. Experimentally PIV is used to measure the local scale displacement fields, and they are used to characterize the failure envelopes of strip footing-gypseous sand interaction problems. For the first time, such outcomes are generated in terms of the field density and saturated and contaminated with oil products such as kerosene gypseous sand, interference effects of the footings, accounting for the characteristics of sand under static loading environments.

2. Model Loading Tests

2.1. Testing Material

Gypseous sand soil from the Anbar Governorate (Fallujah City), in western Iraq, was used for this experimental study at a depth of 0.5–1 m and the flow chart in Figure 1 shows the test program. The characteristics of the sand were described in the Andrea Engineering Tests Laboratory for traditional tests using the American Society for Testing and Materials (ASTM) guidelines, where the experimentally measured material properties showed the following characteristics: maximum dry density (γ_{dmax}) = 16.93 kN/m^3 and minimum dry density (γ_{dmin}) = 12.53 kN/m^3. In addition, using sieve analysis, the grain size distribution curve was used to be as the following things about sand: D_{10} = 0.075 mm; D_{30} = 0.35 mm; D_{60} = 0.60 mm (10, 30, and 60% of the particles are smaller than the sizes shown); D_{50} = 0.31mm (average size of soil particles); C_U = 6.670; and C_C = 3.26 as illustrated in Table 1. Which shows the soil's particle size distribution curve in Figure 2. The sand received poorly graded sand according to the Unified Soil Classification System [23]. Every model test was carried out at a field relative density of 43.36%, with an average gypsum concentration of 25% [24].

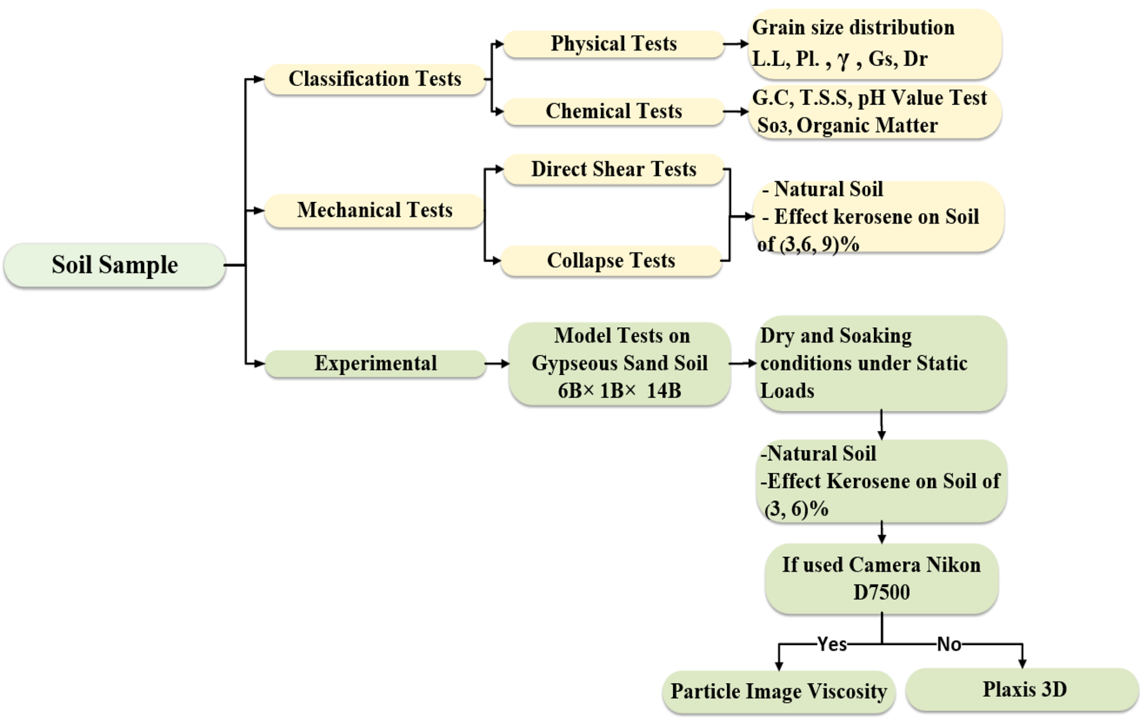

Figure 1. Flowchart of the testing program

Table 1. The summary of physical soil properties

Test		Units	Property	Standard
Natural water content (%)		%	2.14	ASTM D 2216
Atterbergs limits	L.L.	%	39.00	ASTM D 4318
	P.L.		N. P	
	P.I.		N. P	
Specific gravity (Gs)	with water	-	2.37	ASTM D 854-02
	with Kerosene	-	2.35	
In place density, γ_{field}		g/cm^3	1.41	ASTM D 1557
Relative density, Dr		%	43.36	ASTM D 698
Standard compaction test	Maximum dry density	g/cm^3	1.69	
	Optimum moisture content	%	10.94	
The angle of internal friction (ϕ), in dry condition		Degree	35.70°	ASTM D308, 2005
The angle of internal friction (ϕ), in soaking condition			24.90°	
Soil cohesion (c) in the dry		kPa	22.00	
Soil cohesion (c) after soaked			19.33	
Particle size analysis	D_{10}	mm	0.075	ASTMD 422
	D_{30}	mm	0.35	
	D_{60}	mm	0.50	
	Cu	-	6.67	
	Cc	-	3.26	
Passing sieve (0.075 mm)	dry	(%)	12.57	ASTMD 2488
	water	(%)	46.02	
	kerosene	(%)	19.00	
Classification (USCS)	SP (Poorly graded sand with silt)			

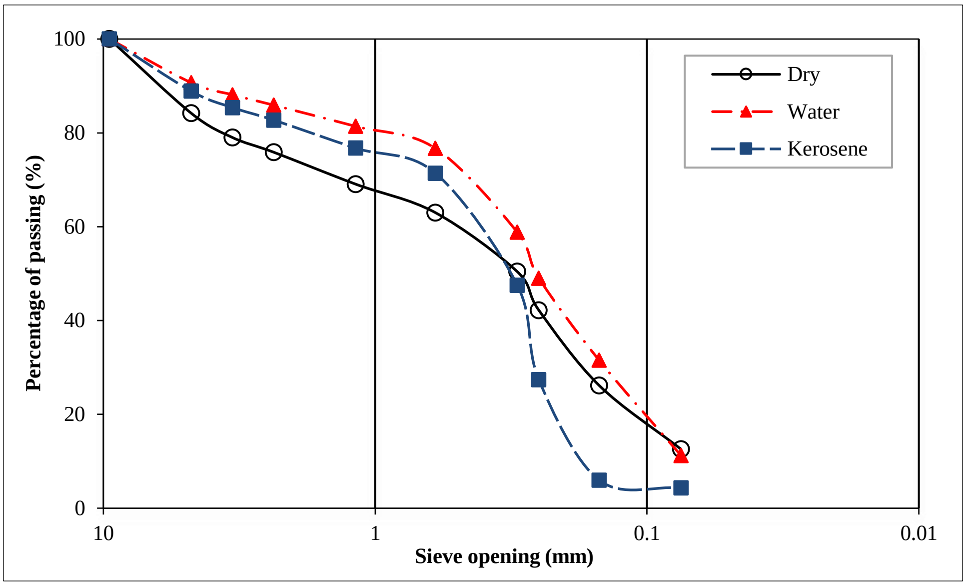

Figure 2. Grain Size Distribution Curves of Gypseous Soil

Furthermore, a compaction test was performed by the ASTM D698 criteria in a conventional manner to extract the highest dry density [25]. It is important to note that in addition to the field density (14.1 kN/m^3), which was verified to determine the density utilized in the test and model sample, close densities in the following proportions were also inferred: 100% (1.69 kN/m^3), 90% (1.592 kN/m^3), and 80% (1.57 kN/m^3). Consequently, the percentage (3%, 6%, 9%) of contaminated kerosene was used to calculate the collapse potential (Cp) of both natural and treated soil. The collapse index of the samples is determined by Equation 1 [26]. Additionally, direct shear tests were performed following [27] specifications for the two conditions (soaked and dry) cases of soil containing 25% gypsum to investigate the impact of the type of oil and the percentage of contamination on the angle of shearing resistance of sand for the soil used in this study. Additionally, tests were performed with a shear displacement rate of 1.25 mm/s and at the same relative density, Dr of 43.36%, and carried out under standard stress conditions of (100, 200, 400) kPa. According to Babalola [28], on clear and contaminated sand, the angles of friction.

$$Cp(\%) = \frac{\Delta H}{H_0} = \frac{\Delta e_0}{1+e_0} \tag{1}$$

This Equation 1 refers to was ΔH change in the height of the sample resulting from wetting to H∘ the initial height of the sample and equals Δe change in the void ratio of the sample resulting from wetting to e∘ natural void ratio. Moreover, the soil condition and tendency to collapse are summarized as shown by Jennings & Knight [29] as a step to finding out the severity of the collapse: Inability to collapse 0-1%; medium collapsibility 1–5%; high collapsibility 5–10%; very high collapsibility 10–20%; extremely collapsible >20%.

2.2. Test Equipment

A steel tank that is 700 mm long, 700 mm wide, and 700 mm high, along with a steel base built to meet both optical and mechanical criteria, is the apparatus used for the model tests as shown in Figure 3. Thus, the model box was spaced apart by an iron material spacer that measured 700 mm in length, 75 mm in width, 700 mm in height, and 10 mm in thickness. With its 15 mm thick glass front, the sample could be seen during preparation, testing gypseous sand deformations could be observed, and friction between the sand particles and the tank wall was reduced.

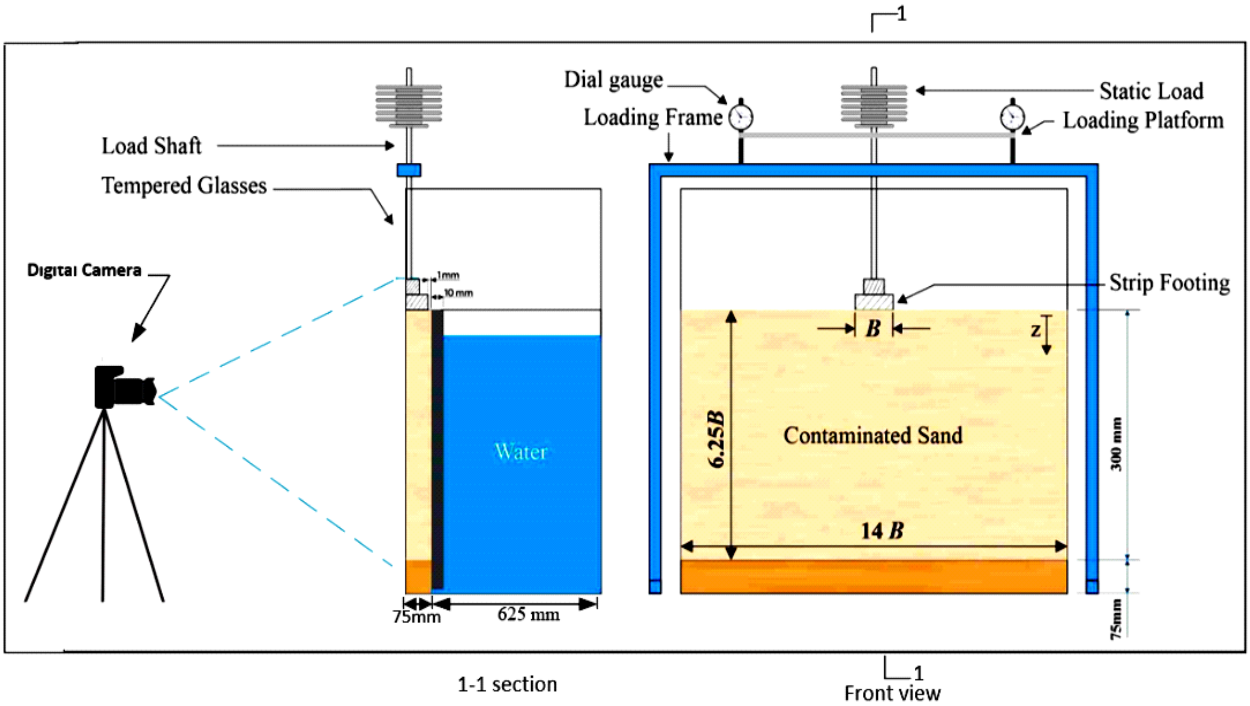

Figure 3. A schematic drawing of the model test setting in millimeters

The inside fixed walls of the tank are polished smooth to reduce friction with the sand as much as possible. Plane-strain conditions were considered for all model tests, therefore, the rigid footing was made of a rigid steel plate with 50 mm in width ×74 mm in length ×25 mm in thickness, note that the length of the foundation is approximately equal to the width of the separator the tank of 75 mm, and the base was relatively rough [30]. The relationship between the angle of interfacial friction of the solid base and the angle of internal friction of the gypseous sand is 0.6-0.7 according to the material used [31]. When the footing width (B) to the average grain size (D_{50}) ratio is 161, it falls within the permitted range and minimizes any size effect that may arise from the footing's various widths and the sand grains' B/D_{50}>100 ratio [19, 21, 29, 32,33]. In light of the aforementioned information, a 1 mm space was created between the iron separator plate and the footing's back to lessen the impact of any frictional forces that may exist between these surfaces. All trials were carried out with the footing on the sand surface ($D_f = 0$). The vertical load was imparted to the model strip footing using a rigid loading structure as shown in Figure 3.

2.3. Kerosene Properties and Contaminated Sand Preparation

Table 2. provides a summary of the essential oil properties tested in the experimental study using a single type of oil and kerosene. Prior to testing, the gypseous sand was carefully mixed with a single type of crude oil at a content of 3%, and 6% oil to ensure homogeneity and consistency. Additionally, the weight of the dry gypseous sand was used to

compute the percentage of oil, which was then combined with the specified weight of 22215 g of dry gypseous sand and added to a steel model. The test model was developed in several stages:

Table 2. Summary of oil properties

Type of oil	Kinematics viscosity ($10^{-6} \times m^2/s$)	Density (kN/m^3)	Specific gravity
kerosene	1.02	8.335	0.785

The purpose of the first stage's 75 mm bottom coarse sand filter layer at the base of the box model was to guarantee both the flashing of air bubbles for the under-soil sample and the even distribution of moisture throughout the soil mass during soaking conditions. In contrast, the second step of sample preparation involves filling the container with well-mixed sand. This was accomplished by layering the sand in multiple layers, one-layer thickness 100 mm, to attain the necessary density along the depth with a satisfactory level of homogeneity. To ensure that the mass of sand grains laid in the box corresponds to the required height and the packing density of the sand, the sand was placed using a load-bearing column affixed to the footing of 5 kg weight, averaging 15 blows per layer, and controlled by pouring the sand into the box using the falling pouring technique method at a constant rate [21, 32, 34]. To guarantee appropriate contact between the compressed layers, the top surface of the sanding bed is also levelled, and each layer is gently set using a hand scraper that has been expressly created for this purpose. As a result, the packed sand was given a full day to settle and compact. Finally, the sandbox was ready, and using the load shaft and disk putty seen in Figure 3, the footing was positioned symmetrically on the surface of the compacted medium-dense gypseous sand layer beneath the loading platform. Before the loading process began, the Nikon D7500 camera was positioned using a camera tripod to eliminate vibrations in front of the viewing window.

2.4. Footing-Sand Interactions with DPIV: Static Load–Mechanisms

The dead load tests were conducted using the static load pattern. Measurements of the footing's collapse potential (Cp) and associated settlement (Su) were made through experiments. It was also done in order to facilitate studies on the mechanical response of the footing-sand interactions. Furthermore, during the trial run, the static load was added one at a time every hour, exactly as the consolidation loads of 25, 50, 100, and 200 kPa that were employed in the current investigation. When loading, a loading stand is utilized to prevent the loads from shifting. A mild axial compression force was applied to the base with the assistance of the load shaft. The tests demonstrated how the medium-density sand took up the footing's load. As required by ASTM D-5333 [35], weight was applied to the sample every hour until its stress reached 200 kPa in dry conditions, readings were obtained using a dial gauge every hour, and photos were taken using a camera every ten seconds. When a load of 200 kPa was applied, the reading was obtained after a full day of testing using the two dial gauges and taking photos. It was completely a period not exceeding an hour, water level was raised in a tank separate from the sandbox. Then, the camera ran and took photos until the model was completely saturated, then readings were taken, and pictures were taken every 10 seconds after 24 hours had passed of sample saturation. Although scale effects from the footing model are known to affect strength estimates, they could be minimized [9, 10]. The model was used to study how the full-size foundation works in real life for small-scale models, the results of tests with laboratory models and the prototype could be different [36].

The model is tested on sandy gypseous soil under harsh conditions, both dry and soaking. It is significant to note that the steel container was left in soaking conditions for a whole day to guarantee that the soil was thoroughly soaked and saturated from soil mixed with various presentations of kerosene material. The test findings are examined for three experimental models. The foundation is positioned in the same vertical line as the container's center of gravity, with care taken to preserve the system's center of gravity. As shown above, in Figure 3, two dial gauges with an accuracy of 0.01 mm/div (50 mm journey) were used to model static load settlement.

2.5. Particle Image Velocimetry (PIV) Theoretical

To study the behavior of sand particles under different conditions using digital photographing and particle image velocimetry (PIV), photos are taken every 10 seconds in dry and saturated condition from soil plane during deformation by high-speed camera, note with dividing the photos into sets and ignoring the first and last sets to guarantee obtain the least amount of noise of sets when the camera is turned on and off, respectively. And then soil deformation is evaluated between each pair of photos and designing the overall images into small sections in the form of squares with the appropriate number of pixels to show the movement of the particles through the PIV analysis. After observing the images of the particles between the two images. According to feature in the program that takes the appropriate squares and not exceeding the sections taken to take the best movement of granules and comparison.

The images were taken using the Nikon D7500, note that camera lens was focused on the 260 mm by 460 mm plane of the footing structure-soil interface area. Since DPIV is an optical method that doesn't change the medium, it can be used to find the flow fields of both fluid and particle media [15, 18]. Some of the things that affect how accurate and good the velocity readings are the size of the picture, the resolution of the pixels, and the rate at which the frames are taken. The image size was 5600 by 3700 pixels, so that the whole footprint of the footing model would be recorded in each frame. To improve the accuracy of the displacement readings, a high pixel resolution of 21.41 by 8.06 pixels/mm was used. Then the images were analyzed through the PIV method using the GeoPIV module. The output of this code is a two-dimensional matrix with u and v components, which represent horizontal and vertical components of the displacement vector in each point, respectively [20, 32].

2.6. Finite Element Method (FEM)

A finite element software called Plaxis 3D was developed by Brinkgreve & Vermeer [37] to analyze the stability and deformation of geotechnical engineering scenarios. Numerous geotechnical issues, including retaining walls, slopes, deep excavations, tunnels, earth constructions, and foundations, can be handled using Plaxis. A three-dimensional nonlinear finite element program has been used to describe a strip footing under a constant load, assuming planar strain conditions [4, 38]. The model's performance was examined, and the model footing is believed to be on the gypseous sandy soil of two types, natural and contaminated, that extends approximately four and a half times as wide from each side. Figure 4 shows the model geometry and fine meshing of the strip-footing system with the footing width B = 50 mm, t = 25 mm, and sample height = 300 mm, which were made to match the lab model using the planar section separated in the tank. Furthermore, it's unclear how well the normalized scale displacements of gypseous sand media match the experimentally measured pattern of gypseous sand particle displacement in footing-gypseous sand interactions—for example, when DPIV is used, as in this study. To match the lab sample, the characteristics of gypseous sand were incorporated into the model Table 3. Then the fully automatic mesh-generation process that divides the geometry into elements is incorporated into the computer program utilized in this investigation. Plaxis offers five different mesh densities, from very coarse to very fine. Using the five global mesh coarseness levels that are currently accessible, some initial calculations were done to determine which mesh would work best for this project. Given that the results for various mesh configurations do not significantly differ, the medium mesh distribution that was optimized for this study and all of the investigations was chosen [39].

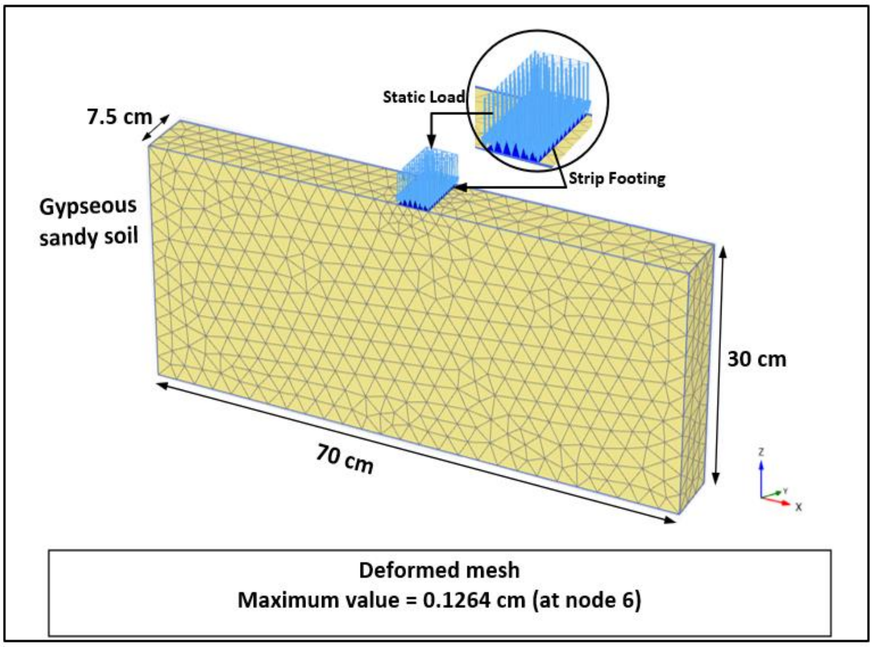

Figure 4. Geometry and meshing for tests of footing width, B = 50 mm

To represent the nonlinear characteristics of gypseous sand, the Mohr-Coulomb model, similar to earlier studies [11, 13] a linear and flawlessly elastic framework, was applied. It was postulated that the sand stratum possessed appropriate plan dimensions, and the depth was represented in the Plaxis model through the utilization of the borehole option. The parameters utilized in the numerical analysis are detailed in Table 3. The assumption was made that the soil was desiccated and that the plate elements were impermeable. Despite the absence of an investigation into the impact of constitutive soil model type on behavior prediction, this study corroborates the model's suitability [40]. The granular soil model was selected to represent the displacement of strip footing due to its ability to capture the increased rigidity in strip footing caused by confining pressure. A vertical load is exerted on the surface of the foundation. For the analysis, the loading point of the soil model is chosen. Plaxis 3D provides a range of procedures that can be utilized to address nonlinear plasticity issues. All procedures are predicated on the selection of step size automatically. Load advancement to the ultimate level is one of the procedures. Primarily, the automated step size procedure is applied to calculation phases that require the attainment of a specific ultimate burden level. The calculation is terminated by the procedure either upon reaching the specified burden level or upon detecting soil failure. A crucial characteristic of this computational process is that the values of the overall burden to be exerted are determined by the user. The input values of a distributed burden in Plaxis 3D are expressed as force per area. The global external burden is ascertained through the utilization of total load multipliers. The final applied load after the calculation phase is determined by multiplying the input load value by the corresponding total load multiplier, assuming neither discharge nor a collapse mechanism occur earlier. Furthermore, a 3D plane strain numerical model is developed using 10-node tetrahedral elements, and various soil elements are considered to be the fundamental components of the 3D finite element mesh (4511). In addition, using a finite element simulation to describe the soil volume precisely, PLAXIS 3D uses a total of 4511 tetrahedral soil elements, each with ten nodes.

Table 3. Input parameters for plane strain condition of the FEM program

Parameters	Gypseous sandy soil	Strip footing
Material model	Mohr-Coulomb	Linear Elastic
Material behavior	Drained	Elastic
Unit weight, γ_{unsat}, kN/m^3	14.1	78.5
Unit weight, γ_{sat}, kN/m^3	18.2	_
Young's modulus, E, kN/m^2 soil natural and soil treated of 3% 6%, respectively [41]	15000, 1350, 14000	200.0E6
Poisson's ratio, ν	0.30	0.26
Cohesion, c, (kN/m^2) natural and treated soils of 3% and 6%, respectively	10, 2.5, 1.49	_
Friction angle (°) in natural and treated soils of 3% and 6% respectively	35.7, 33.6, 35.07	_
Ditalatancy angle, ψ (°) in natural and soils treated of 3% 6%, respectively	0.9, 3.6, 5.07	_

3. Result and Dissection

The work was divided into two parts; the first part included non-contaminated soil from dry to soaking state, while the second one also included contaminated soil with kerosene from dry to soaking state for different percentages:

3.1. Direct Shear Test Results for Contaminated Dense Gypseous Sand Soil

The findings indicated that the angle of internal friction for soil containing 25% gypsum increased from 32.07^0 for the untreated soil to 35.07^0 when 6% kerosene was added. As the percentage of kerosene increases, the angle of internal friction decreases. Soil cohesion increases from 27 kPa for natural soil to 31.8 kPa when 3% kerosene is added to the soil; it decreases from 14.8 kPa to 27 kPa when 6% kerosene is added; and it returns to 14.8 kPa when 6% kerosene is added. A significant influence of kerosene on the angle of internal friction of 25% gypsum-containing soil is observed; the angle of internal friction increases from 32^0 for untreated soil to 35^0 when 6% kerosene is added to the soil. As shown in Table 4. the soil cohesion decreases from 27 kPa to 14.8 kPa when 6% is added. A decrease in soil cohesion and a substantial rise in the angle of internal friction can be attributed to the sharpening and clumping of soil particles caused by kerosene. By increasing the angle of internal friction, the physical bonds between soil grains are also resolved, thereby regulating soil cohesion. The findings are illustrated in Figure 5.

Table 4. Values of Angle of Friction and Cohesion of Sand with Kerosene Content

Dr %	Kerosene%	Dry condition		Saturated Condition	
		ϕ (°)	c (kPa)	ϕ (°)	c (kPa)
43.36%	0.0	32	27	32.975	27.77
	3.0	33.6	31.8	35.04	18.24
	6.0	35.07	14.8	34	22.87
	9.0	32	27	36.132	7.76

3.2. The Effect of Kerosene on Gypseous Sandy Soils Through Collapse Test

Gypseous sand soils were tested in the lab ahead of time and checked with the test single-dimensional compression used for natural soil to find the collapse potential, and the ratio (Cp) was 5.217%. This means those soils have High collapsibility (5–10%) soil accordingly; therefore, it is important to treat these soils to reduce their compressibility characteristics. Moreover, where also, single-dimensional compression was conducted on treated soil. The soil density used in this test is the natural density, equal to 14.1 kN/m^3 and the initial void ratio e_o =0.629 with the natural moisture content. In addition, the results showed that the collapse potential decreased from 5.217% in the natural soil to 2.84% in the soil treated with 6% kerosene, and the collapse potential decreased to 0.95% at the percentage of Kerosene 9%, considered the ideal percentage which gave the smallest value of the collapse potential. Furthermore, the results of elog p are shown in Figure 6, and the variation of collapse potential concerning kerosene content is shown in Figure 7. As the kerosene content of petroleum increases, the collapse potential decreases, as shown in the data. In the case of the uncontaminated sample, saturation has caused the cementing material (gypsum) to dissolve between the gypseous soil particles, resulting in the disruption of interparticle bonding and the rearrangement of particles; this signifies the soil's collapse. The application of kerosene effectively isolates water from contact with gypsum, resulting in a minimum collapse potential value of 9% Kerosene.

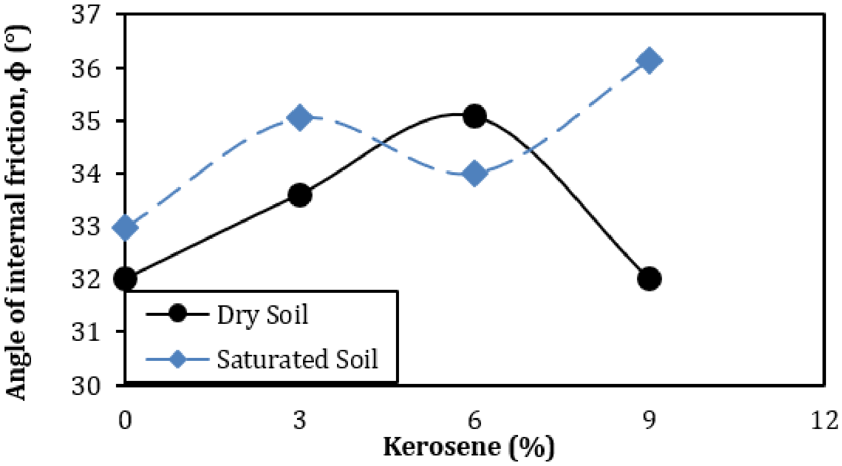

(a)

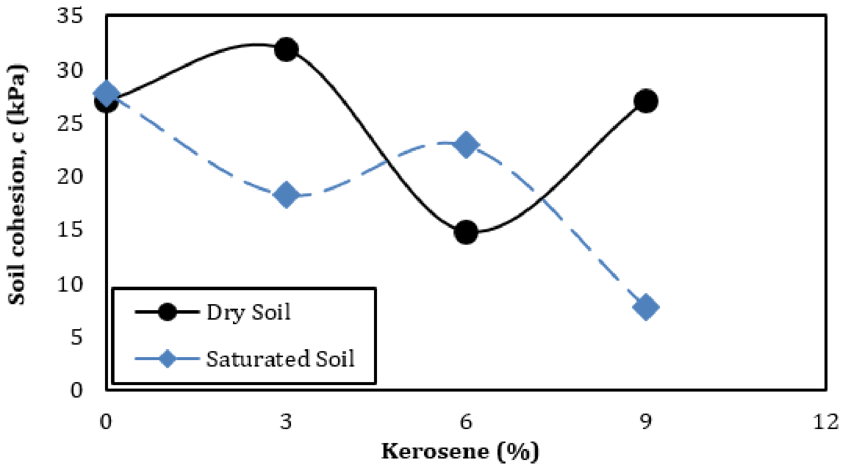

(b)

Figure 5. Direct shear test (a) Friction angle (ϕ), (b) Cohesion (c) of soil with kerosene oil

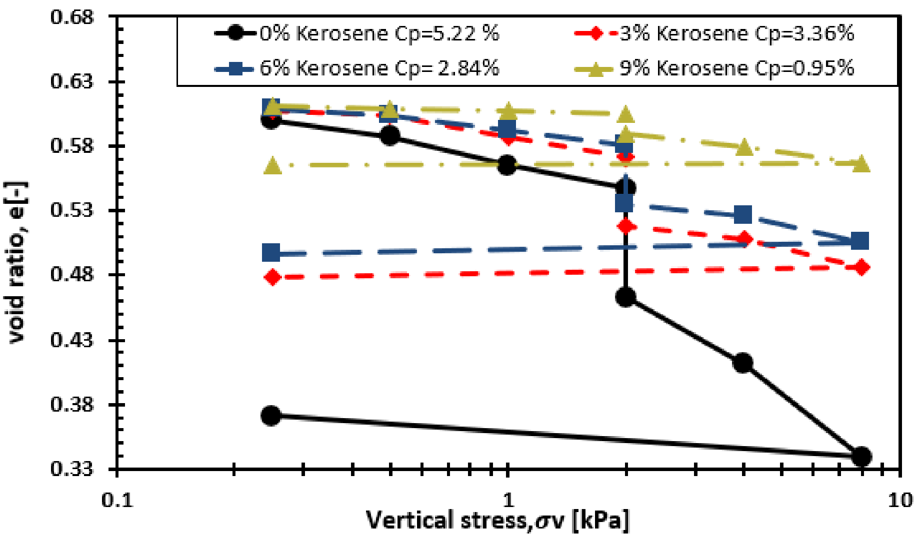

Figure 6. Single collapse test, Cp of model test on soil with kerosene

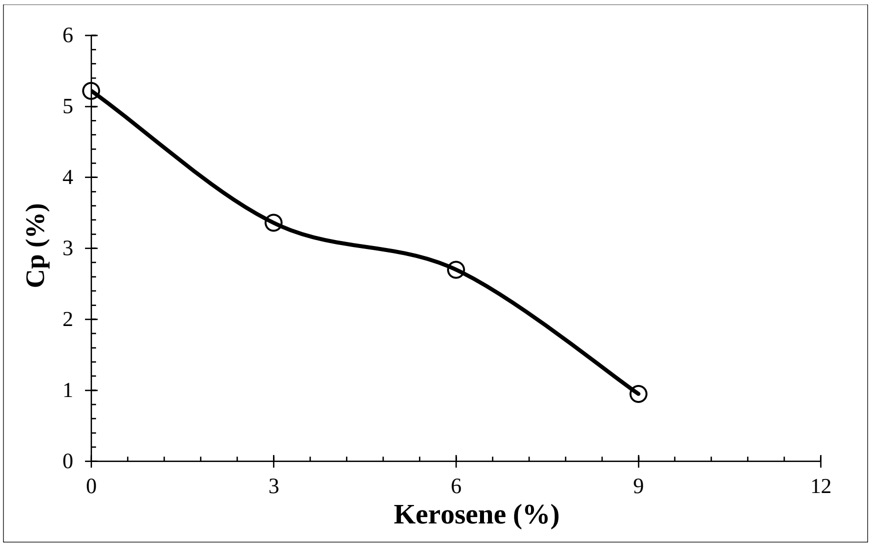

Figure 7. Results of Cp of model test on soil with kerosene

3.3. Load-Settlement Curves from Plaxis and Laboratory Model Tests Are Compare

Figure 8 explains the ratio of ultimate settlement of footing (S) to beam width (B), S/B, in the dry state, is 3.56% for 24 hours, and in soak for 24 hours (S/B) is 40.24%. However, in comparison with Plaxis 3D in dry and soaking conditions, S/B is 2.49% and 38.41%, respectively, which can be consistent with the model soil in the lab. Note that the collapse potential in the test is 6.11% according to Equation (1) in Section (2). Where The soil condition and tendency to collapse were found as a step to finding out the severity of the collapse, which is within the allowed range of high collapsibility (5–10%); therefore, it is important to treat these soils to reduce its compressibility characteristics. Studies have shown that the collapse potential for gypseous soil increases when the water content increases due to a reduction in the matric suction of the soil. But when adding Kerosene in proportions 3,6 %, It makes the soil more solid, which reduces the collapse potential gradually. Therefore, the probability of a collapse was compared at 3% and 6%, where the probability of collapse decreased by 1.48% at 6% compared to 3%(which was 5.4%); in addition, the small value of the collapse that is obtained for percentage 6 % kerosene model is related to many factors such as density condition, high compaction, capillary tension and cementing agent (Kerosene) between soil particles, all these reasons make soil strong and more rigid against collapse so, it is considered a processed material. Upon loading application, there is a gradual increase in the settlement for all models note is the chart to the ratio of ultimate settlement of footing (S) to beam width (B), S/B, in two states (dry, saturated) decrease so that present material kerosene inters particle gypseous sand soils as shown the Figures 9 and 10 Furthermore, after removal of the load, the soil begins to expand to retrieve its initial condition and therefore, the soil volume increases and the expansion value reaches a constant value with time depending on the density, gypsum content and compressibility of soil.

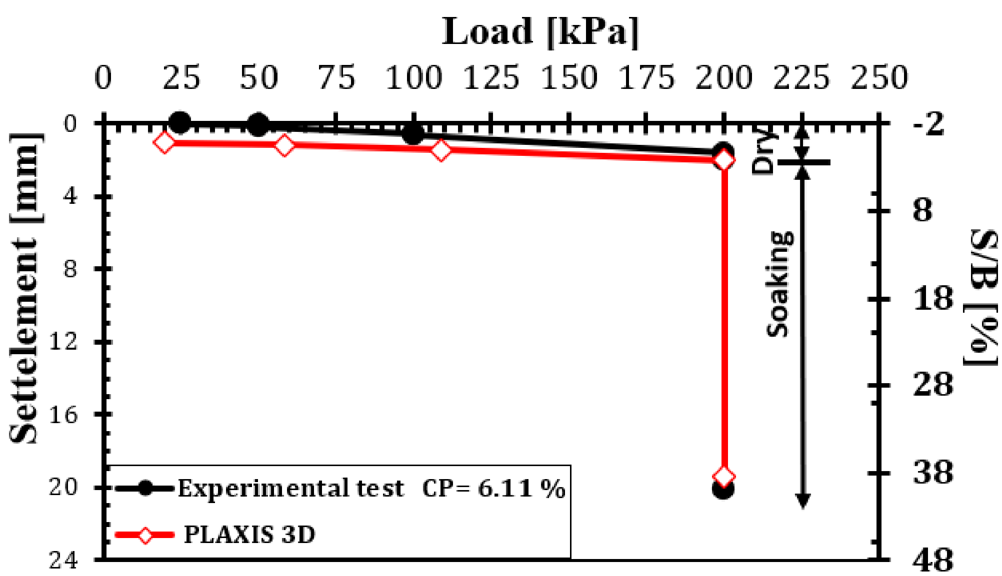

Figure 8. The load-settlement curve of strip footing on medium-dense gypseous sand

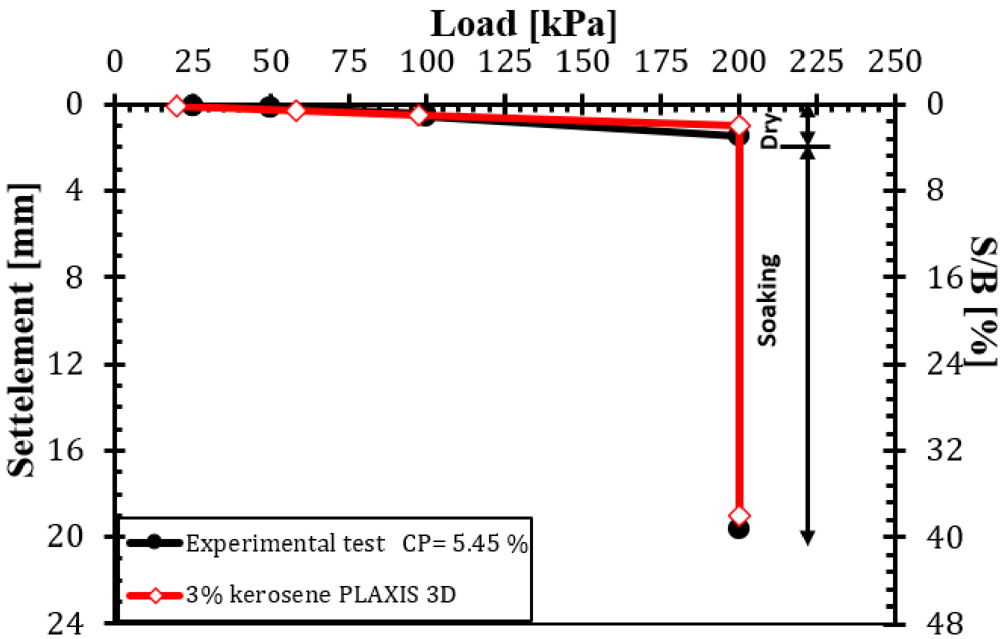

Figure 9. Load-settlement curve of strip footing on medium-dense gypseous sand with 3% kerosene

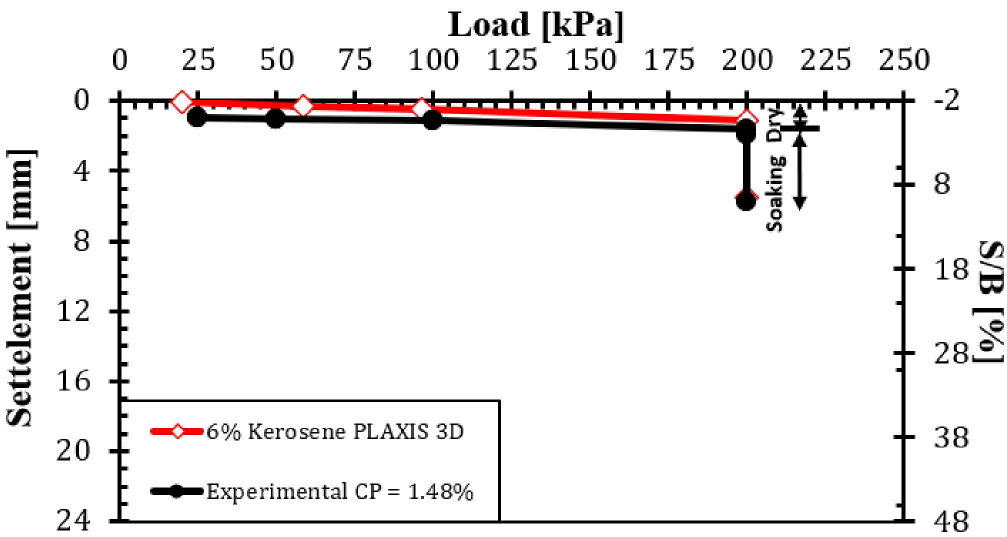

Figure 10. The load-settlement curve of strip footing on medium-dense gypseous sand with 6% kerosene

3.4. Effect of Kerosene on Gypseous Sand: Mean Resultant Velocity Vectors

The PIV program shows a typical evolution of the resulting velocity vectors of the settlement of the strip base located on medium-dense gypseous sand in the loading plate. In the context of program analysis, the statistical vector map is employed to visualize the velocity field of the particles being studied for mean resultant velocity vectors beneath a rigid strip footing subjected to static load. Therefore, this representation allows researchers to observe movement patterns within the soil, including areas of high velocity (such as shear bands) and areas of low or zero velocity (such as stationary regions). Depending on this, PIV analyses were used to determine the speed pattern of the non-contaminated soil and contamination under the loaded footing. According to Prandtl's classical slip-line theory, the soil at the limit state can be split into three zones for dense sand or two zones (Zones I and II) for loose to medium-dense sand. Two tests are conducted, including the first test of untreated soil from dry to soaking state and the second test by treated gypseous soil with percentages from Kerosene of 3% and 6% from dry to soaking states, considering the field density. Depending on the above theory, results in test 1 found that the velocity pattern of non-contaminated soil of Kerosene, after analysis and comparison in zone I, was remarkable, as shown in Figure 11-a. Therefore, particles outside region 1 tend to move downward symmetrically until the final collapse is reached. This study observes similar trends in some states of matter [42-44].

The depth of this plastic wedge when carrying the end bearing was equal to about B, as its vertices (sliding planes) intersect the horizontal at an angle (β) of about (ϕ<β=23.4°< π + ϕ/2) [21, 32]. These are consistent with the Terzaghi [42] assumption of a comparatively approximate basis, which was not confirmed with microscopic experiments for gypseous sandy soil. In addition, Velocity vector maps were the major output of adaptive PIV analysis, which represents the gypseous sand packing and are monitored over time for varying loading levels. The study notes gypseous sand soil speed patterns through previous studies lead to punching shear failure [8, 42, 46]. Despite the difference in types of soil, there is agreement found in comparison with the results of the program for the previous state-of-the-art works, where Jahanger et al. [32] through analysis of soil speed their findings were confirmed after comparison with the Prandtl failure was appeared in local shear failure and punching shear failure for one of sand soil used is loose sand as shown in Figure 11-b. Moreover, Braim et al. [45] studied three different locations of loading were created which were located at the center, 0.05 B and 0.1 B, from the center with respect to the width of the footing to investigate the eccentricity effect applied from the footing. Where one of three locations was compared (at the center) with this work, it was found a clear soil movement to down and right to the left according to Prandtl failure called general shear failure. Therefore, kinematically admissible and mathematically correct theories to describe the complex behavior of granular medium such as PIV and/or the FEM have been adopted as significant methodologies for the researchers in this field.

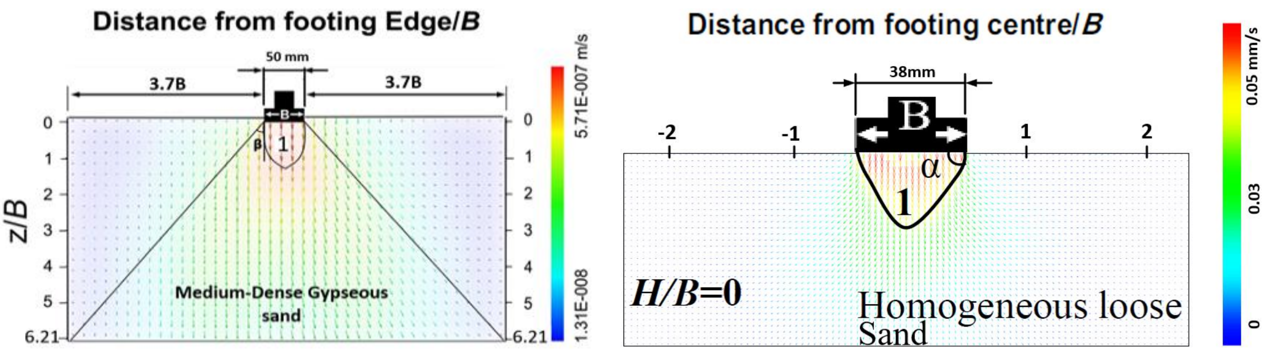

(a) (b)

Figure 11. Evolution of the mean resultant velocity vectors under ultimate bearing capacity (a)beneath strip footing, B=50mm, (b) below strip footing, B = 38 mm [32]

As for test 2, the first percent equal to 3% kerosene for non-contaminated soil treatment was used in test 1. These results are shown in Figure 12, in which a large treatment in PIV analysis was performed with a percentage of 3% kerosene. This led to the emergence of active and passive failure zones (zones 1–3), which are called general shear failure according to Prandtl [46]. The authors also showed that as the particles were outside of zone 1, they tended to move symmetrically downward and to the sides until the maximum load capacity was reached. It was compared with this percentage of 3%, and there was a noticeable convergence in the results in zones (1-3). Other cases were written about [42, 44, 46]. At 6% kerosene, it appeared that the density (additive percentage) of kerosene was very high compared to 3% kerosene, which led to soil saturation for a longer period in the case of soaking gypseous sand soil. Keeping the camera for a longer period, exceeding 5 hours, is difficult due to the presence of devices and equipment adjacent to it, which caused some disturbances during an examination. Also, the 6 % kerosene is oversaturated in the soil.

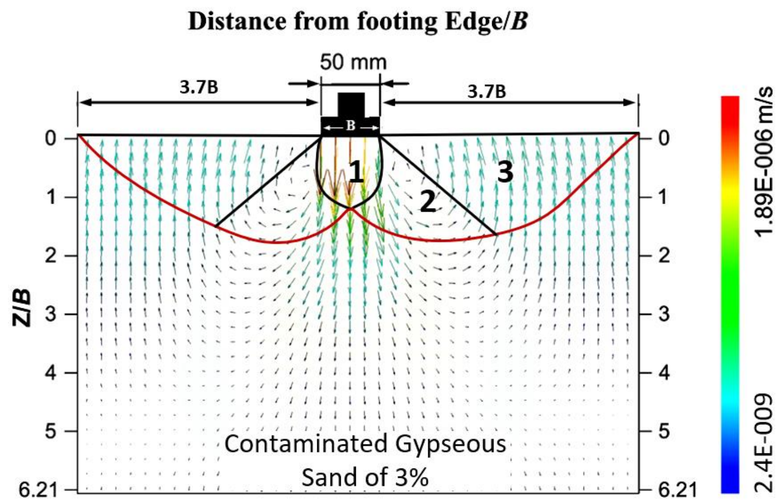

Figure 12. Evolution of the mean resultant velocity vectors medium-dense gypseous sand with 3% kerosene beneath strip footing subjected under stress level 200 kPa. Active dead zone (1), radial shear zone (transition zone) (2) and passive Rankine's zone (3).

3.5. Mean Resultant Displacement Vector: Kerosene Effect Using PIV and PLAXIS

Presents the DPIV-based measures of the mean resultant displacement (with the direction in which they act) under the ultimate load after saturating the system from the bottom; soil deformation was dominated by a vertical consolidation of the gypseous sandy soil; two tests were conducted to examine the behavior of soil based on its moisture conditions. The first test involved an untreated soil sample from a dry state to be soaked. In the second test, the gypseous soil sample was treated with two percentages, the first 3% kerosene, and then soaked from a dry state. The field density must be taken into consideration when conducting these tests. Where the results of the first test of the vertical soil movement can be clearly shown, and the magnitudes (colored plots) and vectors of the incremental displacements in the time steps of the experiment (between 24 hr. of the dry state and 24 hr. of the soaking state) show the strongest compression in the gypseous sandy soil model, where the homogeneous deformation pattern was affected by adding loads from 25 to 200 kPa under drought and soaking conditions. Abrupt collapse can occur in gypseous soil when wet [47]. In the case of the rising water table, for different reasons, the softening of gypsum materials that are between the soil particles will occur. In this state, the bonds that the gypsum materials make between the soil particles are broken [48, 49]. But the results for a type of static load in which the scalar outlines of the vertical and horizontal displacements are superimposed on the resultant displacement vector maps are shown in the panels of Figure 13. The image shows whether the failure process in gypseous sand media under which a static load is driven by horizontal or vertical soil displacements. In addition, it is worth mentioning that damage and cracks in the structures are possible issues when water attacks the supporting gypseous soils [50, 51]. This process creates a structure that is "meta-stable" and makes it easier for particles to slide into a denser state. where it can be explained as the reason for the gradual partial rupture of the gypseous sandy soils during the loading process, as its relative density was equal to 43% from type (medium-dense close to loose sand). So, for loose sand at failure, the soil friction angle is higher than at the beginning of loading due to compaction. The opposite is true in the case of sand, as shown in Figure 13, and is supported by medium-dense gypseous sand. While the results of the 3% and 6% contaminated soil with kerosene test of the PIV program, especially the 3% of Kerosene, shows displacement particle gypseous sand soil noticeably, Figure 14 beyond this region, the particles exhibited a symmetrical downward and lateral motion until reaching their final displacement or max collapse potential under static load 200kPa is reached of saturated state. Similar trends were noticed in other studies, for example, in the sand [44], different soil types [52], soft metals [46], and sand of different densities [21, 42].

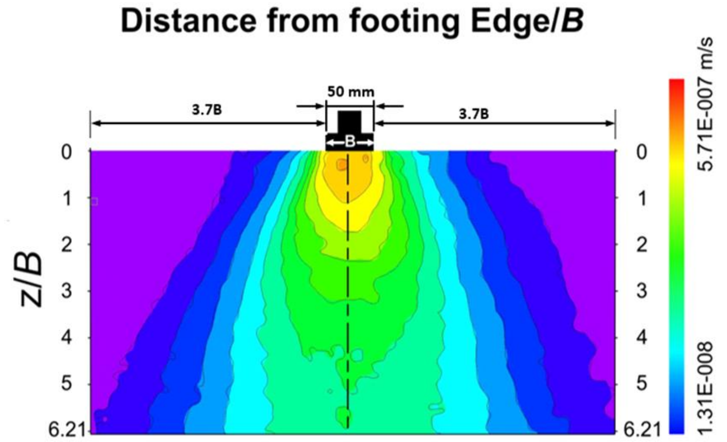

Figure 13. Scalar map of the mean resultant displacement on field gypseous sandy soil using PIV at a stress level of 200 kPa

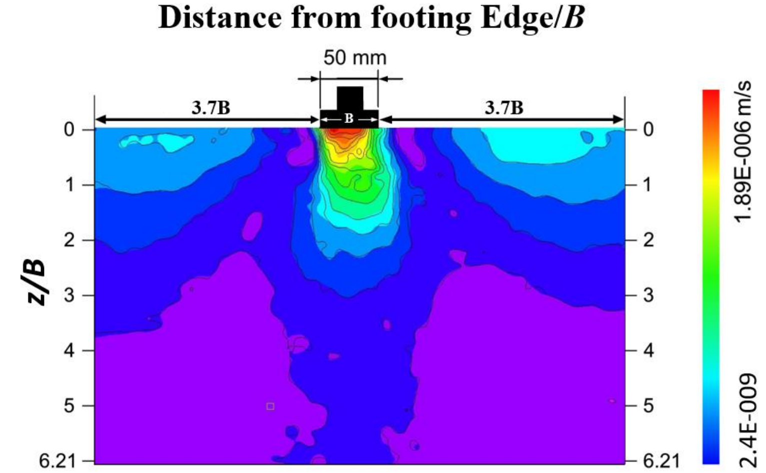

Figure 14. The vertical displacement at a horizontal cross-section 0.5B below the footing on field gypseous sandy soils with added percentages of kerosene oil 3%

Moreover, the results in the first test are close enough but not necessarily the same as those considered in different loading steps in Plaxis analysis as shown in Figure 15. In addition, compared incremental displacements in numerical and laboratory samples were illustrated in Figure 13 with Figure 15. Good agreement can be observed among the obtained results. The marginal disparity in quality, apart from the approximations of computational modeling, may be ascribed to the laboratory lighting conditions and the associated inaccuracies in PIV analysis. In addition, some inconsistencies exist between the displacements calculated by PIV and those generated by numerical simulation. Particle image velocimetry (PIV) has been implemented to measure incremental soil displacement indirectly. From two subsequent images, the incremental displacement field of a moving and deforming soil sample is calculated. They are captured in distinct loading stages that are comparable but not identical to those taken into account in distinct loading stages of the Plaxis analysis. For this reason, the maximal displacements in the PIV analysis surpass those in the Plaxis analysis. Furthermore, it should be noted that the material behavior models implemented in Plaxis are merely simplified renditions of the actual behavior of footing and soil [4].

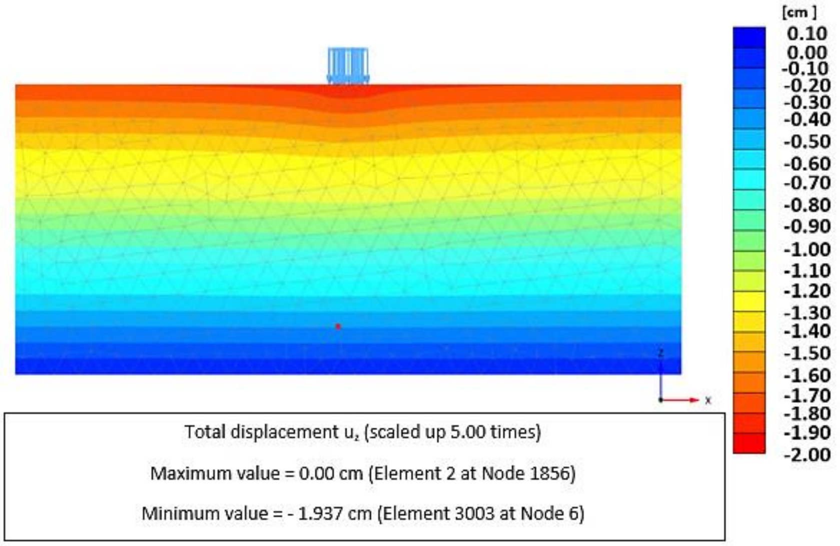

Figure 15. Resultant vertical displacement below the footing for saturated gypseous sandy soil under stress level 200 kPa

In the second test, it appeared that when kerosene material was mixed at a rate of 3% with the field soil, it had no effect on the soil. This is due to the fact that the percentage of kerosene is small. However, when mixing gypseous sand soil with a second percentage equal to 6% kerosene in the lab, we had difficulty capturing images with the camera. Due to the prolonged period of soil saturation, it contains a high percentage of Kerosene, estimated at 6%, which caused us to be unable to analyze the PIV. Therefore, we had to resort to Plaxis 3D software. In addition, Plaxis is a program that can be used instead of the PIV program, which uses a camera to take pictures. Therefore, the Plaxis program above was tested at rates of 0.3%, and its results were compared with the results of my work. The results showed that the Plaxis program is close to the results of my work, and it was also used by Fattahi et al. [38] who indicated that there is a convergence between the results of my work and simulation Plaxis. Therefore, the Plaxis program was used to simulate the percentage of 6% kerosene added to soil, as shown in Figure 16.

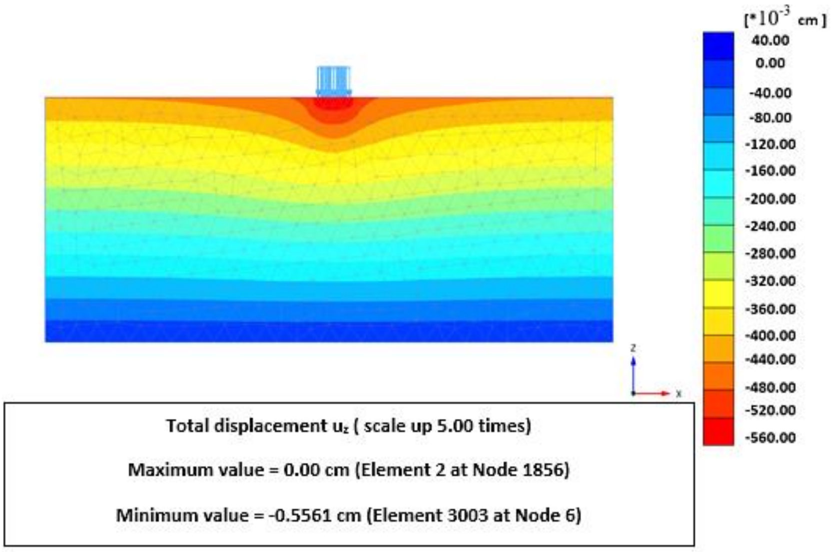

Figure 16. Resultant vertical displacement for the soil of 6% Kerosene under stress level 200 kPa

3.6. Distribution of the Max. Shear Strain Rate Under Maximum Load When Adding Different Percentages of Kerosene Oil

This paper used particle image velocimetry (PIV) to measure the du/dx, and dv/dy strain rates, where over the past three decades, Iraq has dedicated significant efforts to understanding gypseous soils and their behavior in varying environments and under different loads [53]. Various institutions have conducted extensive research programs to shed light on this subject. These research efforts utilized numerical methods to model the dissolving process of gypsum when subjected to soaking and leaching. However, the complexity of gypseous soils has resulted in conflicting results from the vast amount of data gathered through long-term studies, preventing any conclusive decisions. Nevertheless, there has been a particular emphasis on studying the collapsibility and deformability of sandy gypseous soil, with the PIV program being recognized as a more accurate approach in this regard; therefore, two tests were conducted to evaluate the behavior of soil under different moisture conditions using a program PIV. In the first test, untreated soil samples were taken from a dry state and subjected to soaking. In the second test, the gypseous soil sample was treated with two percentages 3 % and 6 % of kerosene, which mixed soil the first 3% of Kerosene was subjected to soaking from a dry state. Also, the gypseous sand soil sample was treatment a second percentage equal to 6% of Kerosene where it is important to consider the field density while conducting these tests. The results of tests show the extent of change gypseous soils change when loads are put on them at different times. The stress rate is highest during soaking in the first test due to the reduced friction and cohesion in the water-saturated soil in which water degrades soil structure, making it more susceptible to deformation, as shown in Figure 17.

Moreover, localized shear bands were characterized by the formation of narrow zones of intense deformation where particles experienced high shear strains. So, the rate at which gypsum dissolves depends on the type and amount of gypsum and environmental changes in moisture content caused by changes in the groundwater table and/or surface water, temperature, permeability, and flow conditions. It is observed that a stress level when the ultimate load (200) kPa has a greater collapse strain when saturated. Therefore, this stress level was chosen for studying the improvement of gypseous soil by oil contamination using 3% and 6% kerosene. When a percentage of 3% kerosene, a high improvement was found in the PIV analysis, as the soil was separated from the water in a soaking state because Kerosene is an insulating material as shown in Figure 18. While DPIV is a dependable and non-intrusive technique for investigating the behavior of granular materials, it is crucial to consider its limits and the scale effects of the model and experimental apparatus. The current study considered this to be using a planar box with dimensions more significant than the footing model. Therefore, further investigation is required to completely grasp the DPIV's limits and scale implications while examining the behavior of granular materials under various loading situations where Particle Image Velocimetry (PIV) was used to investigate the deformation behavior of gypseous soils so that insights into the collapse patterns could be obtained. In contrast to untreated soil, treated gypseous soil exhibits a diminished lacuna ratio due to a reduction in gypsum dissolution, which mitigates strain, as shown in Figure 18.

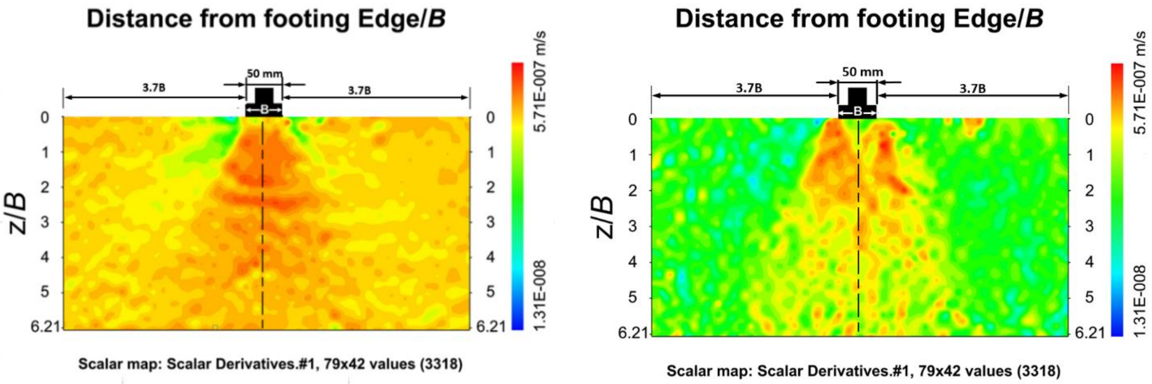

Figure 17. du/dx, (s^{-1}) and dv/dy, (s^{-1}), natural soil under stress level 200 kPa

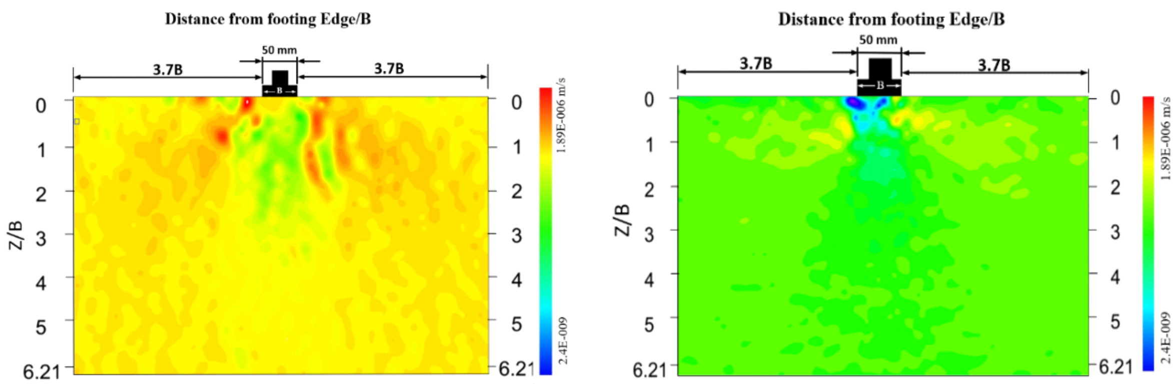

Figure 18. du/dx, (s^{-1}) and dv/dy, (s^{-1}) for 3% of kerosene oil under stress level 200 kPa

As for Plaxis 3D, it was found during the second test that mixing 3% of kerosene into the soil did not show any difference in the cartesian strain. While for the second percentage for the second test, where gypseous sand soil mixed well with equal 6% kerosene, due to the presence of some obstacles during a test period that lasted more than 5 hours to saturate the soil model to contain its high percentage Kerosene that equals 6%, one of these of obstacles such as the camera operating time. The time exceeds 5 hours for the test in only a saturated state under 200 kPa load, where the PIV program could not be used to analyze shear bands. Therefore, FEM was used to simulate untreated (saturated) and treated soil with a percentage of 6% for total cartesian strain, as shown in Figures 19-a, and 19-b. Also, it enhances its resistance to collapse and mitigates the impact of water and subsidence to a certain degree. In this case, the soil collapse pattern was not analyzed by the PIV program, which is why the Plaxis program was noticed to simulate the proportion of this mixture on gypseous sand soil, as shown in Figure 19-b.

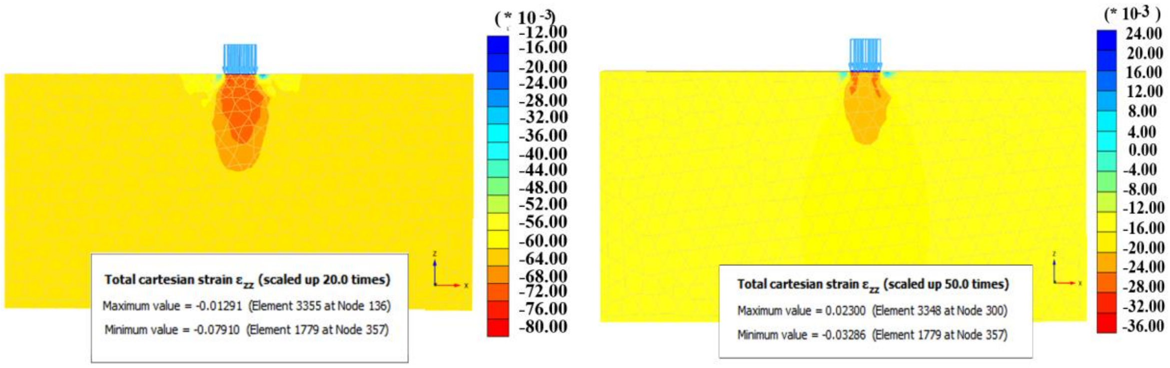

(a) (b)

Figure 19. Total cartesian strain the footing (a) for saturated gypseous sand, (b) after treated 6% percentage of Kerosene under stress level 200 kPa

4. Conclusion

An experimental study was made when using a pollutant, such as kerosene oil, at percentages of 3% and 6%; a difference appeared between the two rates during saturation when taking pictures and analyzing them using the program PIV. A significant improvement appeared in a record period for the gypseous sand soil mixed with 3% kerosene, unlike what appeared for the soil mixed with 6%. Due to the long saturation period, taking pictures was impossible because 6% kerosene was sufficient to isolate water from the soil. This study provides evidence that the PIV is effective for visualizing and characterizing displacement patterns in gypseous sand subjected to static loading. Critical insights into the failure envelope's evolution and distinctive characteristics under the ultimate load can be obtained through the analysis of collapse pattern data, which includes maximal shear strain rate, vertical and horizontal displacements, and vorticity within the gypseous sand. Where the analysis revealed behavior and pattern of untreated field gypsum sandy soil using the PIV program was a downward, symmetrical trend in the particle velocity pattern beyond zone 1, one of-type punching shear failure leading to the ultimate collapse. and PIV's analysis also revealed that the soil particles treated with 3% kerosene demonstrated symmetrical downward and lateral movement until they reached their maximum load capacity. This resulted in the formation of both active and passive failure zones, ultimately leading to general failure. Additionally, results obtained from the numerical models are in good agreement with the experimental results in terms of overall load-settlement behavior and pattern for deformation of gypseous sandy soil interaction strip footing. In all cases, settlement of strip footing obtained from FEM is close to the value obtained from laboratory model tests. The possible differences are due to test errors, soil parameters, or the model used in numerical analyses. Furthermore, it should be noted that the material behavior models implemented in Plaxis are merely simplified renditions of the actual behavior of footing and soil.

5. Declarations

5.1. Author Contributions

Conceptualization, Z.K.J. and H.M.J.; methodology, Z.K.J.; software, H.M.J.; validation, Z.K.J. and H.M.J.; formal analysis, Z.K.J. and H.M.J.; resources, Z.K.J. and H.M.J.; data curation, Z.K.J; writing—original draft preparation, H.M.J.; writing—review and editing, Z.K.J.; visualization, Z.K.J.; supervision, Z.K.J.; project administration, Z.K.J.; funding acquisition, H.M.J. All authors have read and agreed to the published version of the manuscript

5.2. Data Availability Statement

The data presented in this research is available on request from the corresponding author.

5.3. Funding

This research study is funded by Al-Rafidain University College, Baghdad, Iraq.

5.4. Acknowledgements

The authors thank Al-Rafidain University College for their generosity in financial assistance. The authors acknowledge Dr. S. J. Antony, University of Leeds, Leeds, UK, for using PIV software and Andrea Engineering Tests Laboratory, Baghdad, Iraq, for their laboratory equipment.

5.5. Conflicts of Interest

The authors declare no conflict of interest.

6. References

[1] Al-Qhralosy, Z. K. J. (2003). Effect of Cyclic Soaking and Drying on Compressibility Characteristics of Gypseous Soils Stabilized with Emulsified Asphalt. Master Thesis, Al – Mustansiria University, Baghdad, Iraq.

[2] Abood, A. S., Fattah, M. Y., & Al-Adili, A. (2023). Effect of saturation on dynamic characteristics of collapsible gypseous soil using cyclic triaxial testing. Case Studies in Construction Materials, 19, 2502. doi:10.1016/j.cscm.2023.e02502.

[3] Jha, A. K., & Sivapullaiah, P. V. (2017). Unpredictable Behaviour of Gypseous/Gypsiferous Soil: An Overview. Indian Geotechnical Journal, 47(4), 503–520. doi:10.1007/s40098-017-0239-5.

[4] Raee, E., Hataf, N., Barkhordari, K., & Ghahramani, A. (2019). The Effect of Rigidity of Reinforced Stone Columns on Bearing Capacity of Strip Footings on the Stabilized Slopes. International Journal of Civil Engineering, 17(6), 673–685. doi:10.1007/s40999-018-0291-2.

[5] Mohsen, A., & Albusoda, B. S. (2022). The Collapsible Soil, Types, Mechanism, and identification: A Review Study. Journal of Engineering, 28(5), 41–60. doi:10.31026/j.eng.2022.05.04.

[6] Kamil, K. S., Abdulkareem, A. H., & Mahmood, N. S. (2023). Using a Laboratory Model Test to Evaluate Collapsibility of Gypseous Soils Improved by Sludge. E3S Web of Conferences, 427, 1004. doi:10.1051/e3sconf/202342701004.

[7] Abd-Alhameed, H. J., & Al-Busoda, B. S. (2023). Experimental Study on the Behavior of Square-Skirted Foundation Rested on Gypseous soil Under Inclined Load. Journal of Engineering, 29(3), 27–39. doi:10.31026/j.eng.2023.03.03.

[8] Das, B. M. (2019). Advanced soil mechanics. CRC Press, London, United Kingdom. doi:10.1201/9781351215183

[9] Al-Zory, E. A. (1993). The effect of leaching on lime stabilized gypseous soil. Master Thesis, University of Mousl, Mosul, Iraq.

[10] Aziz, H. Y., & Ma, J. (2011). Gypseous soil improvement using fuel oil. World Academy of Science, Engineering and Technology, 51, 299-303.

[11] García Lino, M. C., Pfanzelt, S., Domic, A. I., Hensen, I., Schittek, K., Meneses, R. I., & Bader, M. Y. (2024). Carbon dynamics in high-A Ndean tropical cushion peatlands: A review of geographic patterns and potential drivers. Ecological Monographs, e1614. doi:10.1002/ecm.1614.

[12] Aljuari, K. A., Fattah, M. Y., & Alzaidy, M. N. J. (2023). Behavior of circular skirted footing on gypseous soil subjected to water infiltration. Journal of the Mechanical Behavior of Materials, 32(1), 20220252. doi:10.1515/jmbm-2022-0252.

[13] Ramadhan, R. N., Jassam, M. G., & Jassim, F. H. (2023). Collapsibility and Bearing Capacity of Gypseous Soils Treated with Natural and Industrial Fibers. Solid State Technology, 66(1), 90-110.

[14] Aziz, L. J., & Abdulsatter, S. (2021). the Bearing Capacity of a Circular Footing on Gypseous Soil Before and After Improvement. Kufa Journal of Engineering, 6(1), 57–78. doi:10.30572/2018/kje/611308.

[15] Schröder, A., & Schanz, D. (2023). 3D Lagrangian Particle Tracking in Fluid Mechanics. Annual Review of Fluid Mechanics, 55, 511–540. doi:10.1146/annurev-fluid-031822-041721.

[16] Adrian, R. J. (1991). Particle-imaging techniques for experimental fluid mechanics. Annual Review of Fluid Mechanics, 23(1), 261–304. doi:10.1146/annurev.fl.23.010191.001401.

[17] Lavasan, A.A., & Ghazavi, M. (2016). Failure mechanism and soil deformation pattern of soil beneath interfering square footings. Numerical Methods in Civil Engineering, 1(2), 48–56. doi:10.29252/nmce.1.2.48.

[18] Jahanger, Z. K., Al-Barazanchi, A. J. N., & Ahmed, A. A. (2021). Field Soil Electrical Resistivity Measurements of Some Soil of Iraq. Advanced Geotechnical and Structural Engineering in the Design and Performance of Sustainable Civil Infrastructures. GeoChina 2021, Sustainable Civil Infrastructures. Springer, Cham, Switzerland. doi:10.1007/978-3-030-80155-7_8.

[19] Liu, J., & Iskander, M. (2004). Adaptive Cross Correlation for Imaging Displacements in Soils. Journal of Computing in Civil Engineering, 18(1), 46–57. doi:10.1061/(asce)0887-3801(2004)18:1(46).

[20] Dijkstra, J., Gaudin, C., & White, D. J. (2013). Comparison of failure modes below footings on carbonate and silica sands. International Journal of Physical Modelling in Geotechnics, 13(1), 1–12. doi:10.1680/ijpmg.12.00004.

[21] Jahanger, Z. K., Antony, S. J., Martin, E., & Richter, L. (2018). Interaction of a rigid beam resting on a strong granular layer overlying weak granular soil: Multi-methodological investigations. Journal of Terramechanics, 79(2018b), 23–32. doi:10.1016/j.jterra.2018.05.002.

[22] Al-Obaidi, Q., Mohsen, M., & Asker, A. (2022). Investigation of the Bearing Capacity and Collapsibility of Gypseous Soil Using Geotextile Reinforcement. Engineering and Technology Journal, 40(5), 1–10. doi:10.30684/etj.2021.131076.1002.

[23] Head, K. H. (1980). Manual of soil laboratory testing. Pentech press, London, United Kingdom.

[24] Al-Mufty, A. A., & Nashat, I. H. (2000). Gypsum content determination in gypseous soils and rocks. 3rd International Jordanian Conference on Mining, 25-28 April, Amman, Jordan.

[25] S. Zbar, B., A. Khan, M., & S. Jawad, A. (2013). Geotechnical Properties of Compacted Silty Clay Mixed with Different Sludge Contents. Engineering and Technology Journal, 31(20), 263–279. doi:10.30684/etj.2013.83799.

[26] Shalaby, S. I. (2017). Potential Collapse for Sandy Compacted Soil during Inundation. International Journal of Innovative Science, Engineering & Technology, 4(5), 307–314.

[27] ASTM D3080/D3080M-11. (2020). Standard Test Method for Direct Shear Test of Soils Under Consolidated Drained Conditions. ASTM International, Pennsylvania, United States. doi:10.1520/D3080_D3080M-11.

[28] Babalola, Z. (2016). Direct Shear and Direct Simple Shear Tests: A Comparitive Study of the Strength Parameters and their Dependence on Moisture and Fines Contents, 1–114.

[29] Jennings, J. E., & Knight, K. (1975). A guide to construction on or with materials exhibiting additional settlement due to collapse of grain structure. International Journal of Rock Mechanics and Mining Sciences & Geomechanics Abstracts, 12(9), 131. doi:10.1016/0148-9062(75)91203-6.

[30] Antony, S. J., & Jahanger, Z. K. (2020). Local Scale Displacement Fields in Grains–Structure Interactions Under Cyclic Loading: Experiments and Simulations. Geotechnical and Geological Engineering, 38(2), 1277–1294. doi:10.1007/s10706-019-01088-5.

[31] Galavi, V., Petalas, A., & Brinkgreve, R. B. J. (2013). Finite element modelling of seismic liquefaction in soils. Geotechnical Engineering Journal of the SEAGS & AGSSEA, 44(3), 55-64.

[32] Jahanger, Z. K., Sujatha, J., & Antony, S. J. (2018). Local and Global Granular Mechanical Characteristics of Grain–Structure Interactions. Indian Geotechnical Journal, 48(4), 753–767. doi:10.1007/s40098-018-0295-5.

[33] Cui, M., Chen, F., & Bu, F. (2021). Multiphase theory of granular media and particle simulation method for projectile penetration in sand beds. International Journal of Impact Engineering, 157, 103962. doi:10.1016/j.ijimpeng.2021.103962.

[34] Ekbote, A. G., & Nainegali, L. (2019). Interference of Two Closely Spaced Strip Footings Embedded in Cohesionless Fibre-Reinforced Foundation Soil Bed. Geo-Congress 2019, 454-464. doi:10.1061/9780784482094.041.

[35] Zhang, Y., Hu, Z., & Xue, Z. (2018). A new method of assessing the collapse sensitivity of loess. Bulletin of Engineering Geology and the Environment, 77(4), 1287–1298. doi:10.1007/s10064-018-1372-9.

[36] Vesić, A. S. (1973). Analysis of Ultimate Loads of Shallow Foundations. Journal of the Soil Mechanics and Foundations Division, 99(1), 45–73. doi:10.1061/jsfeaq.0001846.

[37] Brinkgreve, R. B. J., & Vermeer, P. A. (1998). Finite element code for soil and rock analyses. AA Balkema, Rotterdam, Netherlands.

[38] Fattahi, H., Ghaedi, H., Malekmahmoodi, F., & Armaghani, D. J. (2024, June). Accurate estimation of bearing capacity of stone columns reinforced: An investigation of different optimization algorithms. Structures 64, 106519. doi:10.1016/j.istruc.2024.106519.

[39] Boufarh, R., Saadi, D., & Laouar, M. S. (2020). Numerical Investigations on Seismic Bearing Capacity of Interfering Strip Footings. Soils and Rocks, 43(2), 247–259. doi:10.28927/SR.432247.

[40] Kahyaoğlu, M. R., İmançlı, G., Özden, G., & Kayalar, A. (2017). Numerical simulations of landslide-stabilizing piles: a remediation project in Söke, Turkey. Environmental Earth Sciences, 76(19), 1–14. doi:10.1007/s12665-017-6989-7.

[41] Budhu, M. (2010). Soil mechanics and foundations. John Wiley and Sons, Hoboken, United States.

[42] Terzaghi, K. (1943). Liner-Plate Tunnels on the Chicago (Il) Subway. Transactions of the American Society of Civil Engineers, 108(1), 970–1007. doi:10.1061/taceat.0005664.

[43] Yin, J.-H., Wang, Y.-J., & Selvadurai, A. P. S. (2001). Influence of Nonassociativity on the Bearing Capacity of a Strip Footing. Journal of Geotechnical and Geoenvironmental Engineering, 127(11), 985–989. doi:10.1061/(asce)1090-0241(2001)127:11(985).

[44] Murthy, T. G., Gnanamanickam, E., & Chandrasekar, S. (2012). Deformation field in indentation of a granular ensemble. Physical Review E, 85(6). doi:10.1103/physreve.85.061306.

[45] Braim, K. S., Ahmad, S. N. A. S., Rashid, A. S. A., & Mohamad, H. (2016). Strip footing settlement on sandy soil due to eccentricty load. International Journal of GEOMATE, 11(5), 2741–2746. doi:10.21660/2016.27.1344.

[46] Prandtl, L. (1920). On the Hardness of Plastic Bodies. Nachr. Gottinger Nachrichten, 74–85. (In German).

[47] Al-Saoudi, N. K., Al-Khafaji, A. N., & Al-Mosawi, M. J. (2013). Challenging problems of gypseous soils in Iraq. Proceedings of the 18th International Conference on Soil Mechanics and Geotechnical Engineering, 2-6 September, 2013, Paris, France.

[48] Husain, M. M. A., Akhtarpour, A., & Mahmood, M. S. (2018). Wetting Challenges on the Gypsiferous Soils. Proceedings of the 4th International Conference on Civil Engineering, Architecture and Urban Planning, 25-27 July, 2015, Beijing, China.

[49] Abdalhusein, M. M., Akhtarpour, A., & Mahmood, M. S. (2019). Effect of Wetting Process with Presence of Matric Suction on Unsaturated Gypseous Sand Soils. Journal of Southwest Jiaotong University, 54(5), 1-11. doi:10.35741/issn.0258-2724.54.5.3.

[50] Ahmed, K. I. (2013). Effect of gypsum on the hydro-mechanical characteristics of partially saturated sandy soil. Ph.D. Thesis, Cardiff University, Cardiff, United Kingdom.

[51] Fernandes, N. L., Barreto, N. M. B., Machado, A. C., & Rocha, G. P. (2015). Comparative Study between Methodologies Used for Determination of the Total Hardness in Aqueous Matrices. Periódico Tchê Química, 12(24), 91–95.

[52] Terzaghi, K., Peck, R. B., & Mesri, G. (1996). Soil Mechanics in Engineering Practice. John Wiley & Sons, Hoboken, United States.

[53] Mukhlef, O. J., Karkush, M. O., & Zhussupbekov, A. (2020). Strength and Compressibility of Screw Piles Constructed in Gypseous Soil. IOP Conference Series: Materials Science and Engineering, 901(1), 12006. doi:10.1088/1757-899X/901/1/012006.